Journal of Magnetic Resonance **155,** 45–56 (2002)
doi:10.1006/jmre.2002.2504, available online at http://www.idealibrary.com on IDEAL®

Adsorption and Desorption Behavior of NO on H-ZSM-5, Na-ZSM-5, and Na-A as Studied by EPR

Thomas Rudolf, Winfried Böhlmann, and Andreas Pöppl

Fakultät für Physik und Geowissenschaften, Universität Leipzig, Linnéstrasse 5, D-04103 Leipzig, Germany

Received June 22, 2001; revised December 18, 2001

Nitric monoxide probe molecules are used to characterize the Lewis acid properties of sodium cations and aluminum defect centers in various zeolite materials. The adsorption–desorption behavior of NO probe molecules is studied at different temperatures for Na-A, Na-ZSM-5, H-ZSM-5, and silicalite. Adsorbed NO molecules form paramagnetic adsorption complexes with Lewis acid sites which can be examined by EPR transitions ($\Delta m_S \pm 1$) at $g \approx 2.0$. Otherwise the desorption of NO into the gas phase can be monitored by the typical nine-line EPR spectrum ($\Delta m_J \pm 1$) of the $^2\Pi_{3/2}$ state at $g \approx 0.7776$. This gas-phase signal is used to study the overall adsorption–desorption properties of the zeolites in the temperature range $150\,\mathrm{K} \lesssim T \lesssim 300$ K. At lower temperatures the probe molecules are adsorbed at the Lewis acid sites inside the nanoporous materials and produce an intensive spectrum at $T \lesssim 110$ K. But at intermediate temperatures $110\,\mathrm{K} \lesssim T \lesssim 150$ K the NO molecules are adsorbed only for a few hundred picoseconds because the lifetime of the adsorption complexes is limited by the beginning desorption processes. The decreasing lifetime of the adsorption complex with rising temperature results in an increasing homogeneous line broadening of their EPR signals. An analysis of the line-broadening effects provides an opportunity for determining the specific desorption energies E_A(H-ZSM-5) = (20.2 ± 7.3) kJ/mol, E_A(Na-ZSM-5) = (4.1 ± 1.5) kJ/mol, and E_A(Na-A) = (7.1 ± 2.1) kJ/mol for NO probe molecules at sodium cations and aluminum defect centers just below the desorption temperature.

Key Words: **NO adsorption; NO desorption; Na-A; Na-ZSM-5; H-ZSM-5; NO gas phase; Lewis acid surface centers; Arrhenius behavior; X-band EPR; Q-band EPR.**

INTRODUCTION

NO is a suitable probe molecule for studying Lewis acid centers in nanoporous materials such as A type or ZSM-5 type zeolites. In an earlier paper Addison and Barrer (*1*) used NO among other gases such as N_2O, O_2, and Ar to analyze the catalytical activity of zeolites. Later investigation of NO adsorbed in zeolites and on metal oxide surfaces has been extended by electron paramagnetic resonance (EPR) measurements by other researchers (*2–8*). Whereas these papers deal exclusively with the paramagnetic properties of adsorbed NO molecules we now have the opportunity to include additional EPR measurements on desorbed NO molecules. In a recent publication (*9*) we have devised such a method, which allows a detailed characterization of the adsorption–desorption process of NO in zeolite materials by EPR spectroscopy. In this work our approach is used to study NO adsorption at sodium cations in A type, and aluminum defect centers, so-called "true" Lewis acid sites, in ZSM-5 type zeolites. This particular adsorption–desorption method takes advantage of the specific magnetic properties of gaseous NO molecules (*10*) that have been extensively studied by EPR (*11–13*) and microwave absorption (*14, 15*) techniques in the past. It seems worth noting that NO molecules are physically similar to OH radicals (*16, 17*) in terms of their molecular states but are chemically much more stable. Therefore, free NO is easily accessible by EPR spectroscopy.

The NO molecule has one unpaired electron in the diatomic molecular $^2\Pi$ ground state (*10*) with the electron spin $\boldsymbol{S}$ and the orbital angular momentum $\boldsymbol{L}$. The vector coupling of both momenta causes the paramagnetism of this molecule in all states except for the ground state of free NO. The components $\boldsymbol{\Sigma}$ and $\boldsymbol{\Lambda}$ (*10*) of these two angular momenta $\boldsymbol{S}$ and $\boldsymbol{L}$ along the intramolecular axis are antiparallel in the $^2\Pi_{1/2}$ ($J = 1/2, 3/2, \ldots$) states[1] and are parallel in the $^2\Pi_{3/2}$ ($J = 3/2, 5/2, \ldots$) states. The $^2\Pi_{1/2}$ ground state of NO with the total angular momentum quantum number $J = 1/2$ is not paramagnetic. Although the antiparallel components $\boldsymbol{\Sigma}$ and $\boldsymbol{\Lambda}$ of the spin of the electron and its orbital angular momentum have a nonzero resultant total electronic angular momentum $\boldsymbol{\Omega}$ with the quantum number $\Omega = J_{\min} = 1/2$, the components[2] of the *magnetic spin momentum* of the electron and its *magnetic orbital momentum* in the $^2\Pi_{1/2}$ ground state cancel each other and give rise to a zero total magnetic momentum ${}^J\mu_r = 0$, according to Hunds coupling case *a*. But in the $^2\boldsymbol{\Pi}_{3/2}$ state with $J = 3/2, 5/2, \ldots$, the components $\boldsymbol{\Sigma}$ and $\boldsymbol{\Lambda}$ are parallel ($\Omega = 3/2$) and cause the paramagnetism of gaseous NO with a resulting total magnetic momentum ${}^J\mu_r > \mu_B > 0$, where μ_B is the Bohr magneton. The magnetic momentum can be measured by EPR for the lowest $J = 3/2$ level at an electron Zeeman splitting constant $g \approx 0.7776$, and the nine observable EPR transitions are caused by the selection rule $\Delta m_J = \pm 1$, $\Delta m_I^N = 0$. Here m_J and m_I denote the allowed projections of the total

[1] See the notation for diatomic molecules in Herzberg (*10*), $^{2|\Sigma|+1}\Pi_{|\Lambda+\Sigma|}$.
[2] The components along the intramolecular axis of the NO molecule.

1090-7807/02 $35.00

angular momentum $\boldsymbol{J}$ and the nitrogen nuclear spin momentum $\boldsymbol{I}^{\mathrm{N}}$ with $\boldsymbol{I}^{\mathrm{N}} = 1$ onto the quantization axis given by the external magnetic field.

Upon adsorption of NO, $\boldsymbol{S}$ and $\boldsymbol{L}$ are decoupled and the coupling scheme changes completely. We get a paramagnetic complex with an $S = 1/2$ ground state and its g values close to the free electron g value g_e where again the conventional EPR selection rule $\Delta m_S = \pm 1$ holds. This is the EPR transition of interest for the study of adsorbed NO molecules. The paramagnetic properties of the resulting NO adsorption complexes in zeolite materials are described by a conventional spin Hamiltonian

$$\hat{\boldsymbol{H}} = \frac{\mu_{\mathrm{B}}}{\hbar}\hat{\boldsymbol{S}}\boldsymbol{g}\boldsymbol{B} + \frac{2\pi}{\hbar}\hat{\boldsymbol{S}}\boldsymbol{A}^{\mathrm{N}}\hat{\boldsymbol{I}}^{\mathrm{N}} + \frac{2\pi}{\hbar}\hat{\boldsymbol{S}}\boldsymbol{A}^{\mathrm{Al}}\hat{\boldsymbol{I}}^{\mathrm{Al}} \qquad [1]$$

given in energy units. Here $\boldsymbol{B}$ is the magnetic flux density of the homogeneous field, μ_{B} the Bohr magneton, and $\hbar$ Planck's constant according to the values of the CODATA 1999 list (*18*). The quantity $\hat{\boldsymbol{S}}$ denotes the electron spin operator and $\hat{\boldsymbol{I}}^{\mathrm{N}}$, $\hat{\boldsymbol{I}}^{\mathrm{Al}}$ are the nuclear spin operators of the ^{14}N and ^{27}Al nuclei with the corresponding hyperfine (hf) and super hyperfine (shf) coupling tensors $\boldsymbol{A}^{\mathrm{N}}$ and $\boldsymbol{A}^{\mathrm{Al}}$. The evaluation of the hf couplings is essential to determine the electronic structure of the adsorption complex (*4, 21*). The analysis of the principal values of the $\boldsymbol{g}$ tensor of the NO adsorption complexes is based on the formulas of the O_2^- ion in alkali halogenides and is only valid in the limit of an ionic host crystal (*8, 19, 20*). NO and O_2^- have similar electronic structures. In the case of O_2^- the unpaired electron resides in the $^2\Pi_x^*$ orbital while it is in the $^2\Pi_y^*$ orbital for NO. This leads to a change in the sign of the spin–orbit coupling constant λ and exchange of the x and y principal axes of the $\boldsymbol{g}$ tensor (*6, 20*). Then we obtain the following expression for the principal values of $\boldsymbol{g}$ with the NO spin–orbit coupling constant $\lambda = (123.16 \pm 0.02)\ \mathrm{cm}^{-1}$ (*22*)

$$\begin{aligned} g_{xx} &= g_e\frac{\Delta}{\sqrt{\lambda^2+\Delta^2}} - \frac{\lambda}{E}\left(\frac{\Delta-\lambda}{\sqrt{\lambda^2+\Delta^2}} - 1\right) \\ g_{yy} &= g_e\frac{\Delta}{\sqrt{\lambda^2+\Delta^2}} - \frac{\lambda}{E}\left(\frac{\Delta-\lambda}{\sqrt{\lambda^2+\Delta^2}} + 1\right) \\ g_{zz} &= g_e - \frac{2l\lambda}{\sqrt{\lambda^2+\Delta^2}}. \end{aligned} \qquad [2]$$

Here l is a covalency factor and measures the effective g factor of the orbital contribution (*20*) which equals 1 for the free NO molecule and changes slightly on adsorption. The parameters E and Δ define the energy splitting between the $^2\Sigma^*$, $^2\Pi_y^*$ orbitals and between $^2\Pi_x^*$, $^2\Pi_y^*$, respectively, where the unpaired electron resides in the $^2\Pi_y^*$ level. The splitting Δ can be used as a measure for the electric surface field at the NO adsorption site (*2, 6, 20*). However, all three $\boldsymbol{g}$ tensor principal values must be known according to Eq. [2] to determine precisely the splitting Δ together with the parameters E and l, which are given by the solution of a fourth-order polynomial equation. Unfortunately, the orthorhombic distortion $g_{xx} - g_{yy}$ of the $\boldsymbol{g}$ tensor of the NO adsorption complexes is in the order of 10^{-3} or even less but can be resolved by the application of multifrequency EPR spectroscopy at low temperatures in combination with the deconvolution of the experimental spectra. Recently, the potential of this approach has successfully been demonstrated for Na^+–NO complexes in Na-A and Na-ZSM-5 zeolites (*23*).

Whereas EPR measurements at low temperatures are useful for characterizing the adsorbed state of the NO in the zeolite materials, experiments at temperatures above 80 K allow the study of the adsorption and desorption processes of the nitric oxide molecules as shown in a previous paper (*9*). The desorption of the NO molecules from the adsorption sites leads to a drastic decrease in the EPR signal intensity of the NO adsorption complexes with rising temperature and eventually to the total disappearance of their EPR signal. At slightly higher temperatures the desorbed NO molecules in the gas phase above the sample can be monitored by the EPR signal of their paramagnetic $^2\Pi_{3/2}$ molecular state. The appearance of the gas-phase signal defines a characteristic temperature T_{des} of the desorption process. The decrease in the EPR signal intensity of the NO adsorption complexes with proceeding desorption is accompanied by a strong increase in the homogeneous linewidth δB^{hom} of their EPR signal that measures the reciprocal lifetime of the adsorbed state. The homogeneous linewidth follows an Arrhenius behavior

$$\delta B^{\mathrm{hom}}(T) = b_1 e^{-\frac{E_{\mathrm{A}}}{k_{\mathrm{B}}T}} \qquad [3]$$

with the preexponential factor b_1 and the Boltzmann constant k_{B}, which can be used to evaluate an activation energy E_{A} from the temperature dependence of $\delta B^{\mathrm{hom}}(T)$. Above a certain energy E_{A}, the dissociation probability is appreciable. One expects a dissociation rate proportional to $\exp[-E_{\mathrm{A}}/k_{\mathrm{B}}T]$ which is involved as the Arrhenius factor (*24*). The specific values of this energy E_{A} are characteristic for different adsorption sites in the nanoporous materials and have a microscopic character of a desorption energy E_{des} per NO adsorption complex in molar units.

In this work, we study NO adsorption and desorption at Na^+ cations in Na-A and Na-ZSM-5 and at aluminum defect centers (true Lewis acid sites) in H-ZSM-5 type zeolites by X-band EPR spectroscopy. Furthermore, the adsorption complex of NO with aluminum defect centers is investigated by X- and Q-band EPR spectroscopy at low temperatures to obtain more reliable information about the chemical nature of these true Lewis acid sites. The A type zeolite can be characterized by a cubic unit cell built of a strictly alternating –Si–O–Al– network with a silicon to aluminum ratio Si/Al = 1, whereas the ZSM-5 type zeolites have mainly –Si–O–Si– bonds with only a

few –Al– framework sites in the lattice (Si/Al $\approx 15 \ldots \infty$) and a ZSM-5 typical zigzag-like channel system. The interaction of NO probe molecules with Na^+ cations in Na-ZSM-5 and Na-A zeolites and aluminum defect centers in the H-ZSM-5 zeolites will be studied to determine the desorption energies E_{des} of NO at these adsorption sites. The energies E_{des} are expected to be sensitive to the type of adsorption center and may be interpreted as a local acid strength per adsorption site. It is worth noting that both sodium cations and aluminum defect centers posses Lewis acid properties (*3, 25*).

EXPERIMENTAL

The EPR experiments were carried out on an X-band ESR 380 E and on a Q-band EMX BRUKER spectrometer. The B field has been calibrated by the ^{1}H NMR magnetometer MJ110R. For the EPR measurements of the NO adsorption complexes we have used field modulation amplitudes of 0.4 mT for Na-A and Na-ZSM-5 and 0.2 mT for H-ZSM-5. The NO gas-phase measurements have been done at $B_0 \approx 890$ mT ($g \approx 0.7776$) at typical X-band frequencies with a modulation amplitude of 1.0 mT. This overmodulation has been applied successfully to detect also NO molecules in the gas phase at very low concentrations without a remarkable influence on the overall intensity dependence.

The zeolites Na-A, Na-ZSM-5 with Si/Al = 22, and H-ZSM-5 with Si/Al = 15 were synthesized according to standard procedures (*26, 27*) and are microcrystalline powders. The samples have to be prepared at HV conditions $p < 5.0 \times 10^{-7}$ mbar in a 100% steel vacuum line to enable a NO adsorption without O_2 pollution. In this way we can prevent a reduction of NO to $N_2 + O_2$ and N_yO_x. The zeolite samples were dehydrated at the activation temperatures T_{act} (H-ZSM-5) = 800°C, T_{act} (Na-ZSM-5) = 300°C, and T_{act} (Na-A) = 450°C, then treated with O_2 at the same activation temperatures, and subsequently evacuated. Nitric oxide was adsorbed on such prepared samples in defined quantities (gas volume of about 4 ml and pressures of $p_{NO} \approx 0.5$ and 1.0 mbar for Q- and X-band samples, respectively). This is equivalent to $\approx 5 \times 10^{16}$ NO molecules for Q-band and $\approx 10^{17}$ for X-band samples and results in a probe molecule density of about 10^{-1} per unit cell in the nanoporous sieves. An additional pure silicalite sample (ZSM-5 type zeolite with Si/Al = ∞) was prepared at $T_{silicalite} = 800$°C and $p_{NO} = 1.0$ mbar according to the given preparation procedure. For X-band experiments standard EPR quartz tubes with an outer diameter of about 4.0 mm were used. Q-band samples were prepared in a 2.0-mm section for the 34-GHz measurements, which was connected axial symmetrically to an upper 4.0-mm-diameter section for subsequent NO gas-phase measurements at X-band frequencies. The upper 4.0-mm-diameter section of the Q-band sample tubes was necessary to have enough NO molecules at a low pressure in the resonator space in order to obtain narrow and intense NO gas-phase EPR signals.

RESULTS

EPR of adsorbed NO at low temperatures. EPR experiments at $T = 10$ K have been performed to confirm the formation of NO adsorption complexes in the zeolite materials and to characterize their specific structures. Figure 1 illustrates the experimental X- and Q-band EPR spectrum of NO adsorbed on H-ZSM-5 zeolites. The spectra exhibit an anisotropic $\boldsymbol{g}$ tensor and a shf splitting of about 1.1 mT into six fairly well-resolved lines due to the magnetic interaction of the unpaired electron at the nitric oxide molecule with one ^{27}Al ($I = 5/2$) nuclear spin. Comparable spectra have been reported in the literature (*5, 7, 21*) and are typical for NO coordinated to aluminum defect centers. The assignment of the shf splitting to the interaction of the unpaired electron with the aluminum nucleus was proved by pulsed ENDOR spectroscopy (*5*) and may be considered evidence for the direct coordination of NO to an aluminum site. The typical nitrogen hf triplet of the NO adsorption complexes with a splitting of about 3.0 mT along the g_{yy} principal axis (*2–9*) is somewhat obscured by the ^{27}Al shf splitting but can be inferred from the position of the additional aluminum shf components at the low-field edge of the experimental EPR spectra.

The EPR spectra in Fig. 1 have been analyzed on the basis of the spin Hamiltonian in Eq. [1], a first-order perturbation theory approach, and a numerical deconvolution procedure of the experimental spectra as described earlier (*23*). The linewidth model related to g anisotropy of Wang and Hansen (*28*) has been applied in the calculation of the powder patterns. This model uses a lineshape function which is described by a superposition of a Gaussian and a Lorentzian distribution with relative contributions $0 \le r_{LG} \le 1$ of the Gaussian and $(1 - r_{LG})$ of the Lorentzian part. For this lineshape a total linewidth $\delta^{total}B$ related to g anisotropy

$$(\delta^{total}B)^2 = \frac{(\delta^{total}B_x g_{xx} l_x)^2 + (\delta^{total}B_y g_{yy} l_y)^2 + (\delta^{total}B_z g_{zz} l_z)^2}{(g_{xx} l_x)^2 + (g_{yy} l_y)^2 + (g_{zz} l_z)^2} \quad [4]$$

has been defined, where

$$l_x = \cos(\vartheta)\cos(\varphi), \quad l_y = \cos(\vartheta)\sin(\varphi), \quad l_z = \sin(\vartheta) \quad [5]$$

are the direction cosines. The angles φ and ϑ are the polar angles in the unit sphere. The quantities $\delta^{total}B_i$ ($i = x, y, z$) are the linewidths at the g_{xx}, g_{yy}, and g_{zz} orientations.

The determined spin Hamiltonian parameters of the NO adsorption complex in H-ZSM-5 zeolites are given in Table 1. The extracted total linewidths are $\delta^{total}B_{xx} = 5.0$ mT, $\delta^{total}B_{yy} = 0.35$ mT, $\delta^{total}B_{zz} = 8.0$ mT for the X-band spectrum and $\delta^{total}B_{xx} = 5.0$ mT, $\delta^{total}B_{yy} = 0.35$ mT, $\delta^{total}B_{zz} = 7.0$ mT at Q-band frequencies. The computed spectra using these parameters are likewise shown in Fig. 1 for comparison.

The peculiarity of H-ZSM-5 is that the spectral analysis of the experimental spectra has not shown any deviation ($g_{xx} \neq g_{yy}$)

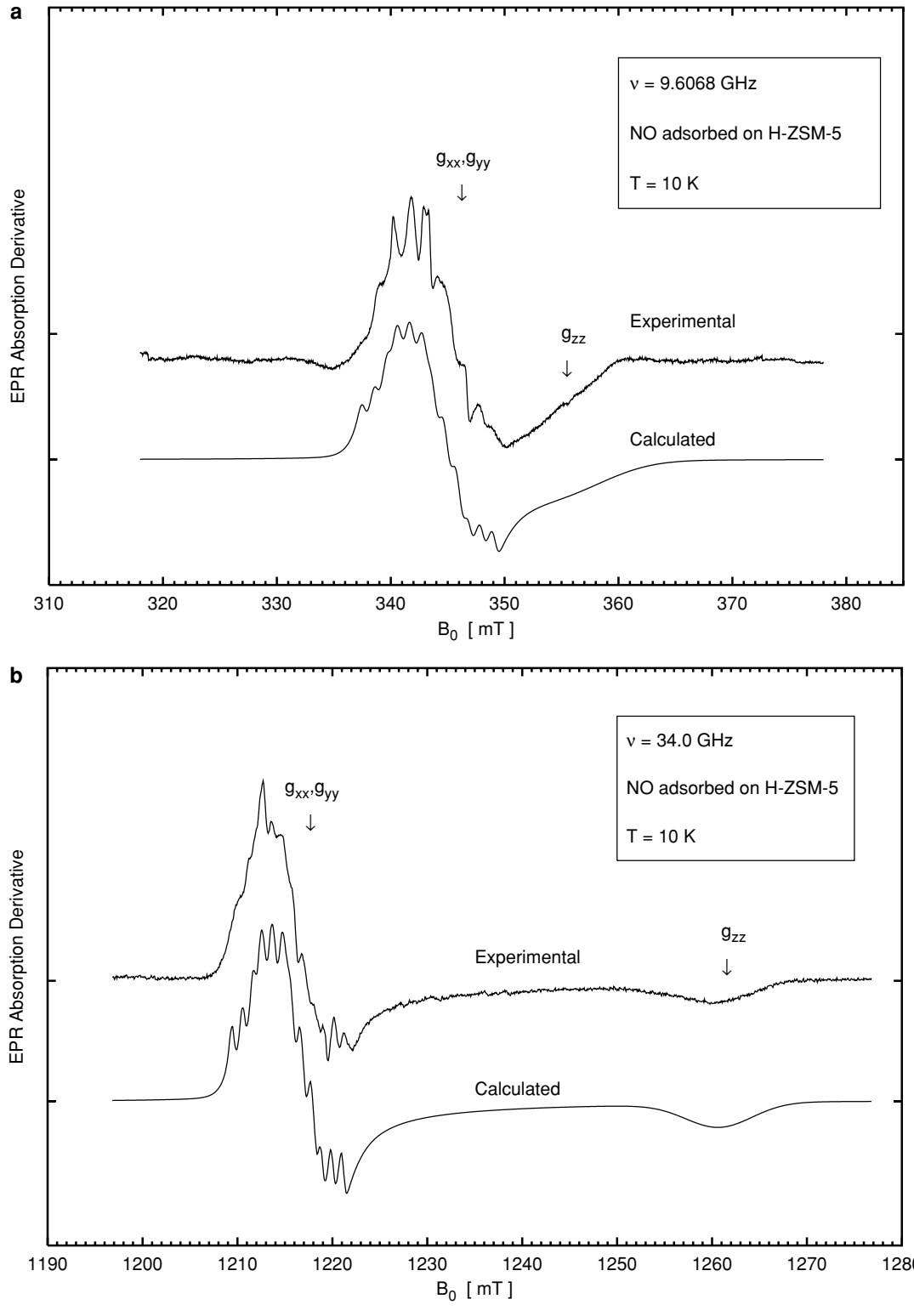

FIG. 1. Experimental and calculated EPR spectra of NO adsorbed on H-ZSM-5 at $T = 10$ K: (a) X-band and (b) Q-band spectra. The marked positions indicate (a) the g_{xx}/g_{yy} and (b) the g_{zz} spectral region.

TABLE 1

Spin Hamiltonian Parameters of the NO Adsorption Complexes, Activation Temperatures T_{act}, Desorption Energies E_A, and Desorption Temperatures T_{des}

NO adsorbed on zeolite matrix:	H-ZSM-5	Na-ZSM-5[a]	Na-A[a]		Silicalite
T_{act} [°C]:	800	300	450		800
E_A [kJ/mol]	20.2 ± 7.3	4.1 ± 1.5	7.1 ± 2.1		No monomer found
E_A [kJ/mol][b]	1.1 ± 0.6				
T_{des} [K]	240	190	150		150
$T_{measure}$ [K]	10	10	10	80	10[c]
g_{xx}[d]	1.999	1.9939	1.9993	1.9795	—
g_{yy}[d]	1.999	1.9914	1.9936	1.9892	—
g_{zz}[d]	1.927	1.8460	1.8842	1.9061	—
A^N_{xx} [MHz][e]	≈0.0[f]	32.5	16.2	31.2	—
A^N_{yy} [MHz][e]	84.1	102.0	91.6	84.6	—
A^N_{zz} [MHz]	≈0.0	≈0.0	≈0.0	≈0.0	—
A^{Al}_{xx} [MHz]	≈0.0	—	—	—	—
A^{Al}_{yy} [MHz][e]	31.2	—	—	—	—
A^{Al}_{zz} [MHz]	≈0.0	—	—	—	—

[a] Spin Hamiltonian parameters were taken from Ref. (*23*).
[b] E_A for a second process with Arrhenius behavior.
[c] Test measurements have been done.
[d] Absolute error is 0.003.
[e] Absolute error for resolved hf and shf interactions is 6.2 MHz.
[f] Some hf and shf interactions could not be resolved and are marked by ≈0.0 which is also the value used for the calculated spectrum.

of the $\boldsymbol{g}$ tensor from axial symmetry for the NO complex in H-ZSM-5. The uncertainty in $g_{xx} - g_{yy}$ was evaluated to be 0.0002 but $g_{xx} = g_{yy}$ best fit the spectra. Furthermore, an aluminum shf coupling could only be determined for the y principal axis of the $\boldsymbol{A}^{Al}$ tensor. This direction is defined by the y principal axis of the nitrogen hf interaction tensor (*2*) with the principal axes value $A^N_{yy} = 84$ MHz. The outer ^{27}Al shf lines belonging to the $m^N_I = \pm 1$ transitions of the nitrogen hf triplet splitting along the y axis are somewhat broadened in both experimental spectra. A reasonable assumption to explain this might be a distribution of the A^N_{yy} principal value of the ^{14}N hf interaction. Although it is a very time-consuming task initial computer calculations have shown that this could be a successful approach for a better fit of the experimental spectra but has not been studied further at this point. For the x and z directions we could not resolve any hf or shf splitting but found surprisingly large linewidths $\delta^{total}B_{xx}$ and $\delta^{total}B_{zz}$ that may account for unresolved ^{14}N hf and ^{27}Al shf couplings.

The spin Hamiltonian parameters of the Na^+–NO adsorption complexes in Na-A and Na-ZSM-5 zeolites at low temperatures have been determined by multifrequency EPR spectroscopy in an earlier work (*23*). The parameters are likewise summarized in Table 1. No sodium shf coupling could be observed in the EPR spectra of both systems. But pulsed ENDOR experiments in Na-A zeolites revealed the ^{23}Na shf interaction to prove the direct coordination of the NO to the alkali metal cation (*4*). Note that an internal motional process within the Na^+–NO complex in Na-A zeolites leads to a partial motionally averaged spectrum at temperatures $T > 40$ K (*8, 9*), which gives rise to a different set of spin Hamiltonian parameters at elevated temperatures (Table 1).

EPR of adsorbed NO at elevated temperatures. NO adsorption complexes are not stable in zeolites at higher temperatures because nitric oxide desorbs at $T > 100$ K. There are two possibilities for studying this desorption process by EPR, either by measurement of the adsorbed state or by monitoring the paramagnetic $^2\Pi_{3/2}$ molecular state of the desorbed NO molecules in the gas phase. Figures 2–4 illustrate the obtained temperature dependences of the EPR intensity of the adsorbed state at $g \approx 2$ and of the $^2\Pi_{3/2}$ state at $g \approx 0.8$ of the desorbed molecules for the samples H-ZSM-5, Na-ZSM-5, and Na-A. The intensities of the adsorbed state are found at the low-temperature side of these plots and have been obtained by double integration of the first derivative EPR signals. For H-ZSM-5 and Na-ZSM-5 (Figs. 2 and 3) the EPR intensities of the NO adsorption complexes decrease continuously with rising temperature between $30 \text{ K} \leq T < 180$ K. The spectrum disappears at about $T \approx 180$ K for both materials. A stronger temperature dependence of the EPR signal intensity is observed for the Na^+–NO complex in Na-A zeolites between $120 \text{ K} \leq T \leq 140$ (Fig. 4) where the EPR signal of the adsorbed state disappears at $T > 140$ K. It should be noted that the relative EPR intensities provide only a rough measure of the concentration of the NO adsorption complexes since they also depend on the temperature-dependent paramagnetic susceptibility and quality factor of the cavity. But the disappearance of the EPR signals at higher temperatures is a strong indication of a substantial decrease in the complex concentration, which is caused by desorption of the NO.

The decrease in the EPR intensity of the adsorption complexes with rising temperature is accompanied by a homogeneous line broadening of their EPR signals as shown from the insets in Figs. 5–7. We determined the homogeneous linewidths δB^{hom} for the three samples at the various temperatures by a numerical deconvolution algorithm. The analysis is based on a least-squares fit of the experimental data using the respective spin Hamiltonian parameters in Table 1 to obtain the total linewidth components $\delta^{total}B_i$. The homogeneous linewidth at the specific temperature was then calculated according to

$$\delta B^{hom}(T) = \delta^{total}B_i(T) - \delta^{total}B_i(T_0). \quad [6]$$

The quantities $\delta^{total}B_i(T_0)$ are the temperature-independent total linewidth components at low temperatures. Note that the total linewidth components and spin Hamiltonian parameters measured at $T_0 = 80$ K were taken in the case of the Na-A zeolite whereas the low-temperature results at $T_0 = 10$ K were used for the samples Na-ZSM-5 and H-ZSM-5. In all cases the analysis provided the same values δB^{hom} for all three components $\delta^{total}B_i$ at a given temperature, which supports the assumption of a homogeneous line-broadening process.

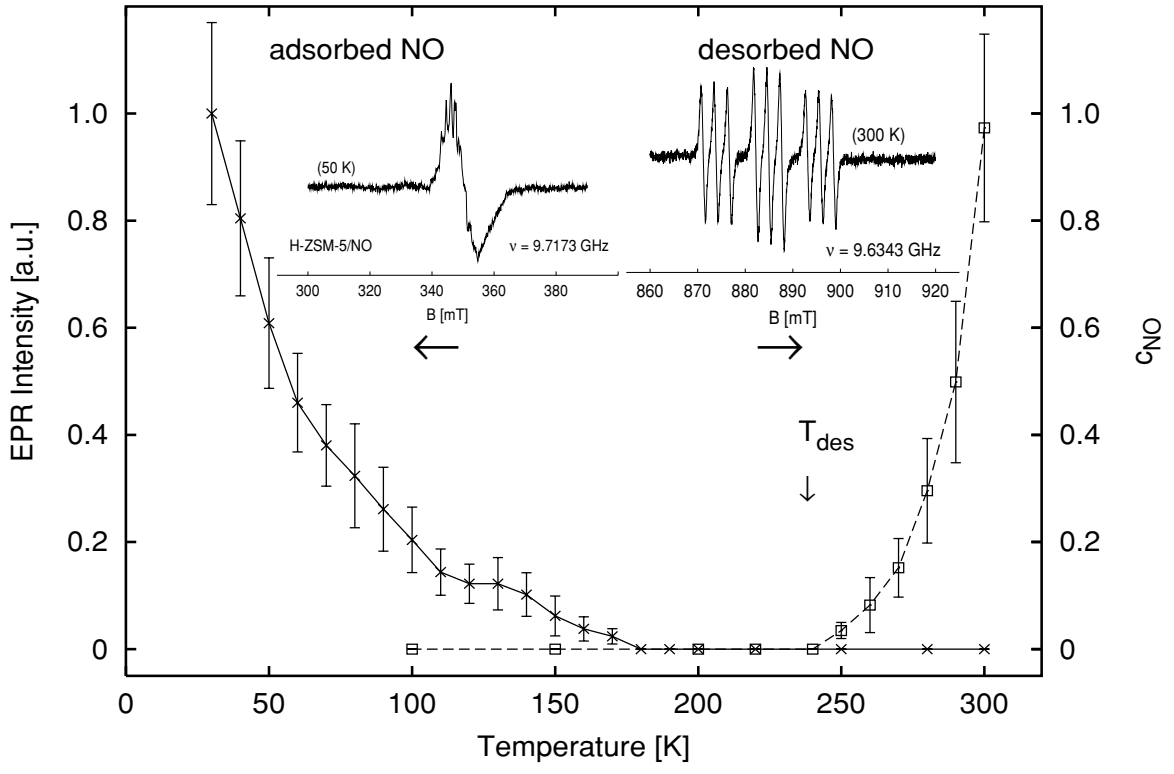

FIG. 2. Adsorption and desorption behavior of NO on H-ZSM-5 with relative intensities of the adsorbed state (×) and relative concentrations c_{NO} of desorbed NO molecules (□).

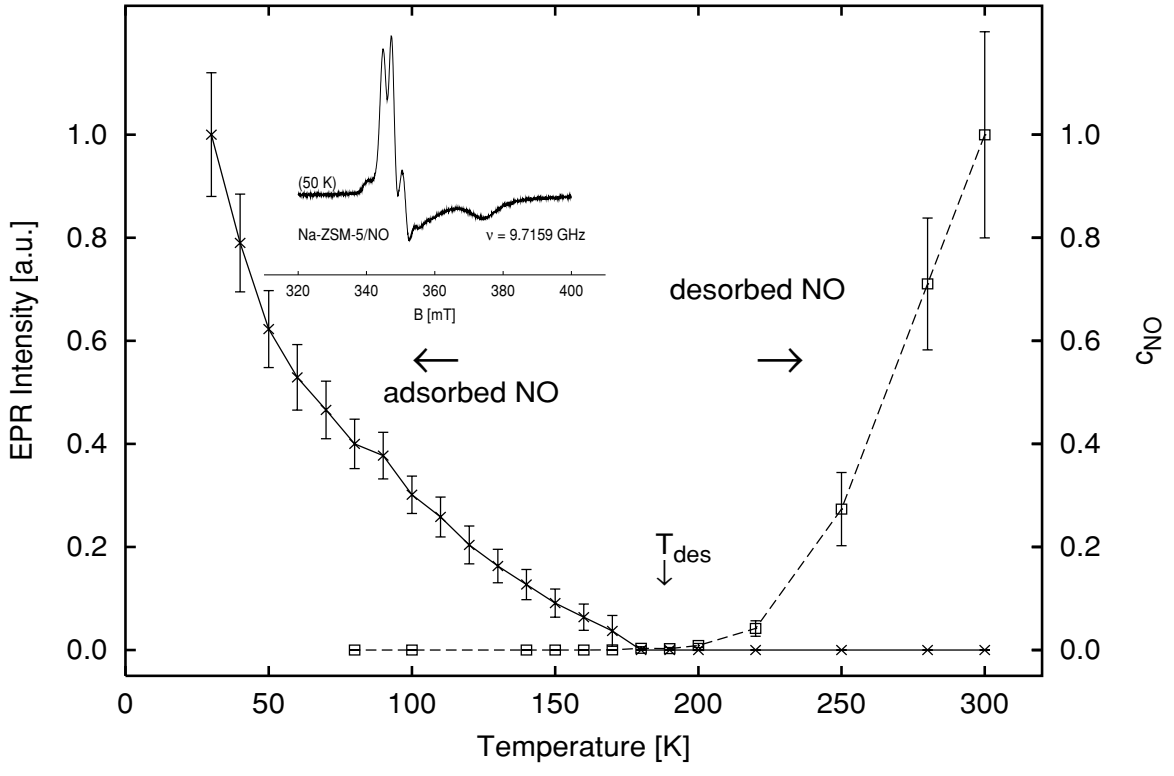

FIG. 3. Adsorption and desorption behavior of NO on Na-ZSM-5 with relative intensities of the adsorbed state (×) and relative concentrations c_{NO} of desorbed NO molecules (□).

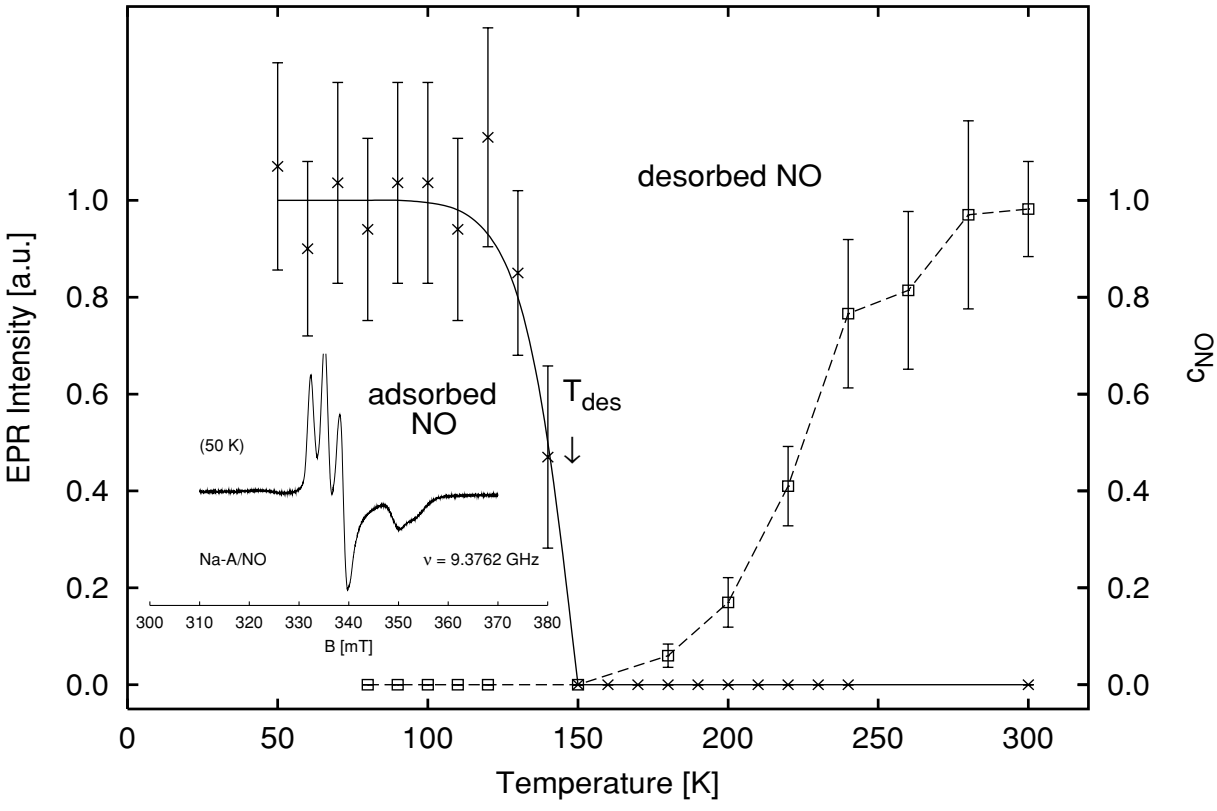

FIG. 4. Adsorption and desorption behavior of NO on Na-A with relative intensities of the adsorbed state (×) and relative concentrations c_{NO} of desorbed NO molecules (□).

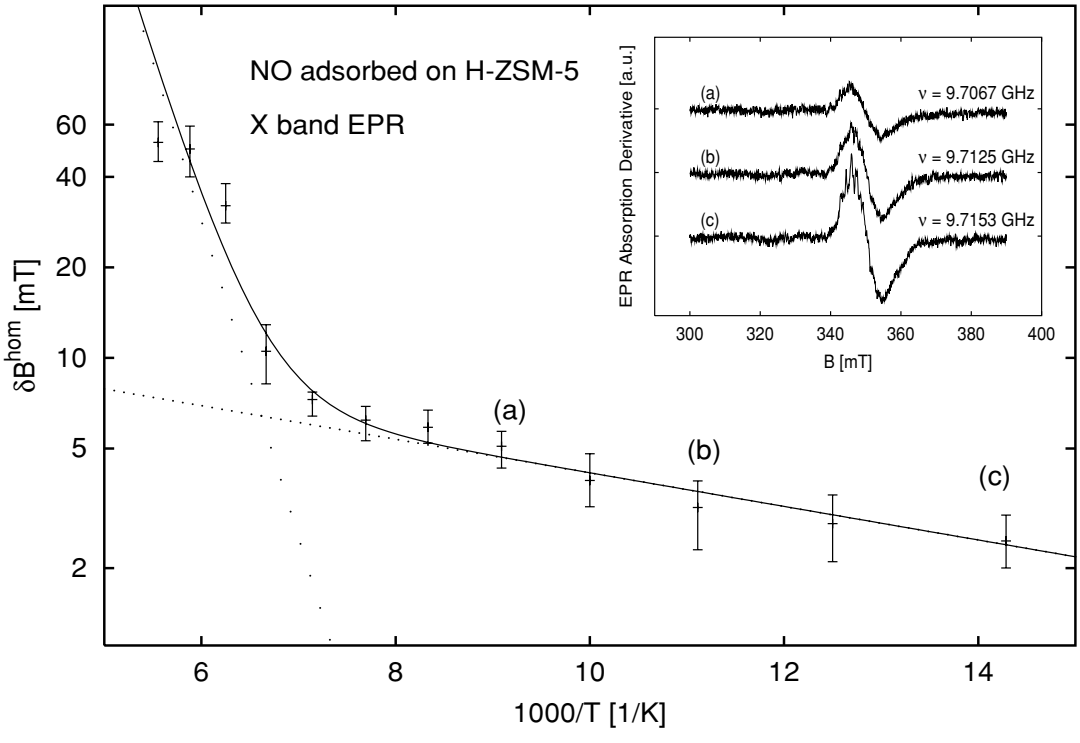

FIG. 5. Arrhenius plot of the homogeneous EPR linewidths δB^{hom} of adsorbed NO on H-ZSM-5. The inset shows the corresponding EPR spectra at (a) $T = 110$ K, (b) $T = 90$ K, and (c) $T = 70$ K.

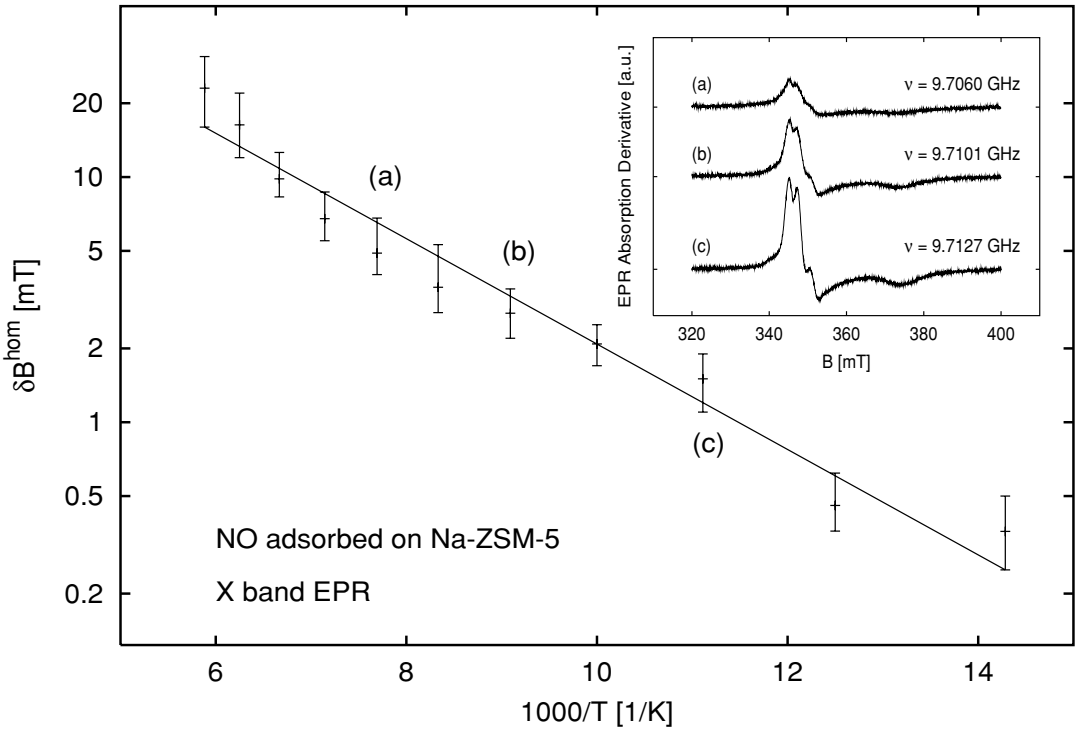

FIG. 6. Arrhenius plot of the homogeneous EPR linewidths δB^{hom} of adsorbed NO on Na-ZSM-5. The inset shows the corresponding EPR spectra at (a) $T = 130$ K, (b) $T = 110$ K, and (c) $T = 90$ K.

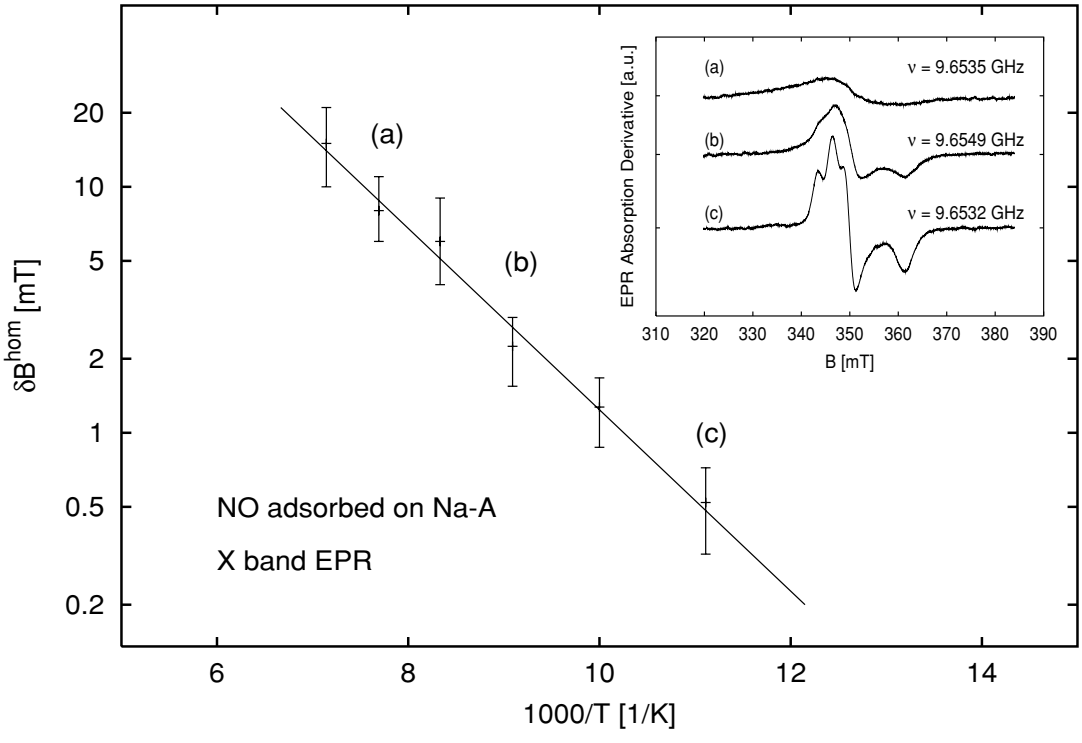

FIG. 7. Arrhenius plot of the homogeneous EPR linewidths δB^{hom} of adsorbed NO on Na-A. The inset shows the corresponding EPR spectra at (a) $T = 130$ K, (b) $T = 110$ K, and (c) $T = 90$ K.

The homogeneous linewidths δB^{hom} obtained as a measure of the reciprocal lifetime of the adsorption complexes were plotted versus the reciprocal temperature in Figs. 5–7. The expected Arrhenius behavior (Eq. [3]) was found for all three samples. The Na-ZSM-5 (Fig. 6) and Na-A (Fig. 7) materials gave each a monoexponential temperature dependence of δB^{hom}, which allowed the determination of a single activation energy E_A. A biexponential behavior was obtained for H-ZSM-5, indicating the existence of two activated processes. Here the high-temperature process with $E_A = 20.2$ kJ/mol is identified as the desorption process of the NO molecules. The determined activation energies are summarized in Table 1.

EPR of desorbed NO. The concentration of desorbed NO molecules in the gas phase above the zeolite materials can be measured by EPR via their paramagnetic $^2\Pi_{3/2}$ molecular state. The rotational ground state ($J = 3/2$) of the $^2\Pi_{3/2}$ molecules provides a characteristic nine-line EPR pattern at $g \approx 0.8$ (inset in Fig. 2). However, the intensity of the EPR signal of the $^2\Pi_{3/2}$ state depends on the NO gas pressure, the paramagnetic susceptibility, and the population of the rotational ground state of the $^2\Pi_{3/2}$ electronic state in a complicated manner. Therefore, we have studied the temperature dependence of the EPR signal intensity of the $^2\Pi_{3/2}$ state in a pure NO gas-phase sample with a total NO pressure of $p_{\mathrm{NO}} = 1.0$ mbar at room temperature. The intensities are again obtained by double integration of the EPR spectra and are displayed in Fig. 8. Later these data were used as an intensity standard to convert EPR intensities of NO gas-phase spectra of zeolite materials into relative concentrations $0 \le c_{\mathrm{NO}} \le 1$ of desorbed NO molecules. It is worth noting that (a) only those NO molecules, which are in the sample volume inside the microwave cavity, contribute to the given intensities and (b) the relative concentrations are calculated as intensity values relative to the intensities given in Fig. 8 and are then normalized by setting the room temperature value to $c_{\mathrm{NO}} = 1$. Finally, we have true NO concentrations where $c_{\mathrm{NO}} = 1$ corresponds to about 10^{17} NO molecules in an X-band sample tube outside the zeolite crystallites. During the experiments it was found that at all temperatures below room temperature we get relative NO concentrations in the range $0 \le c_{\mathrm{NO}} \le 1$. Furthermore, the linewidth of the gas-phase spectrum shows a characteristic dependence on the NO gas pressure. The absolute NO concentration at a given temperature could be calculated from these linewidths. Figure 8 shows that there are no molecules in the gas phase at $T \lesssim 70$ K and the nitric oxide is liquid or frozen. The intensity maximum at $T_{\mathrm{m}} \approx 110$ K defines the temperature where all NO molecules have entered the gas phase. The NO concentration in the gas phase is expected to be constant for $T > T_{\mathrm{m}}$ whereas the number of EPR active molecules may change in dependence on the temperature-dependent population of the $^2\Pi_{3/2}$ ($J = 3/2$) state. It should be mentioned that the temperature T_{m} depends on the freezing point of NO, which in turn is determined by the NO pressure. Thus, T_{m} would decrease for lower pressures.

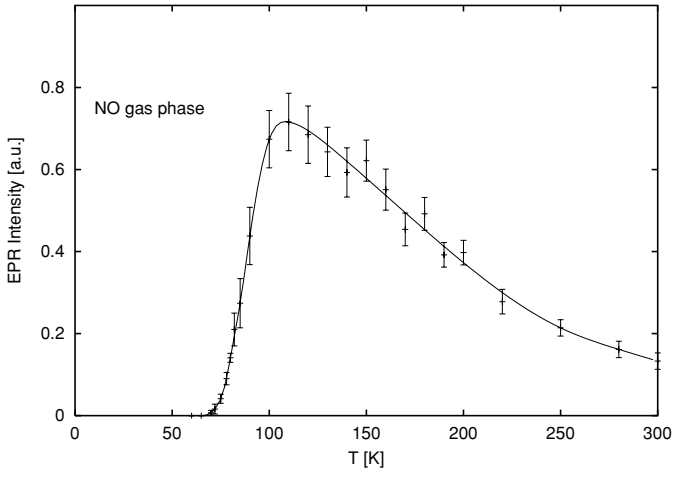

FIG. 8. Temperature dependence of the intensity of the typical nine-line EPR spectra of the $^2\Pi_{3/2}$, $J = 3/2$ state of free NO molecules. The NO has a considerable partial pressure at 77.4 K and can be gaseous at this temperature. The nitrogen monoxide is completely liquid or frozen at $T \lesssim 70$ K and EPR spectra cannot be detected. The intensity decreases at $T > 110$ K because the population of NO in higher excited rotational states $J > 3/2$ increases according to the Boltzmann distribution and the $^2\Pi_{3/2}$, $J = 3/2$ state is then less populated.

The temperature dependence of the intensity of the gas-phase EPR signal of the $^2\Pi_{3/2}$ ($J = 3/2$) state of the desorbed NO molecules was measured for all three zeolite samples H-ZSM-5, Na-ZSM-5, and Na-A. Then these intensities were normalized by the standard intensities from Fig. 8 to yield relative concentrations of desorbed NO molecules. These values are depicted in Figs. 5–7 together with the EPR intensities of the NO adsorption complexes. Obviously the desorption of NO molecules into the gas phase starts at temperatures that are slightly higher than those where the EPR signal of the adsorbed molecules cannot be observed anymore. The relative concentration of desorbed nitric oxide increases continuously with rising temperature. For the zeolite Na-A a maximum of desorbed NO seems to be reached at room temperature whereas no saturation of the desorption process is observed for both ZSM-5 type materials up to temperatures of about 300 K. The desorption temperatures $T_{\mathrm{des}} \approx 150 \ldots 240$ K in Table 1 define the highest temperatures where gas-phase EPR signals cannot be detected. At temperatures $T \le T_{\mathrm{des}}$ the NO molecules are completely adsorbed by the zeolite materials. The lowest desorption temperature was obtained for the sample Na-A in accordance with the observed maximum in the relative concentration of the NO gas-phase molecules at room temperature. Furthermore, we have to note that NO in Na-A and Na-ZSM-5 samples is chemically stable over a period of months. In contrast, NO in H-ZSM-5 materials decomposes at room temperature within a couple of days as indicated by the disappearance of the EPR signals of both adsorbed state and gas phase. This instability varies strongly depending on the preparation conditions but was not the subject of this work.

The desorption properties of NO in a pure silicalite sample (Si/Al $= \infty$) were also investigated for comparison. This

material does not contain Lewis acid sites that give rise to paramagnetic NO adsorption centers. Therefore, adsorbed NO molecules could not be detected by EPR. But the gas-phase EPR spectrum showed that NO molecules are likewise completely adsorbed at $T \leq 150$ K in this ZSM-5 type material.

DISCUSSION

Lewis acidity of adsorption sites and NO desorption. Nitric oxide possesses Lewis basic properties and can be used as a probe to characterize the electron pair acceptor strength of Lewis acid adsorption sites in zeolite materials such as sodium cations (weak Lewis sites) and aluminum defect centers (strong Lewis sites). In this approach the interaction strength between the NO molecules and the adsorption sites is taken as a measure for their Lewis acidity (*3*). Information about the interaction strength can be gained from an EPR study of the NO desorption behavior. The experiments in Figs. 2–4 showed that NO molecules desorb above different temperatures T_{des} depending on the type of adsorption site and zeolite. At temperatures $T \leq T_{\text{des}}$ they are completely adsorbed within the zeolite material as indicated by the disappearance of the NO gas-phase signal (Figs. 2–4). Just below T_{des} neither the gas phase nor the signal of the adsorbed NO state is observed. The nitric oxide molecules are expected to diffuse through the nanoporous channels where they are only adsorbed at the Lewis acid sites for a limited period of time ($<10^{-10}$ s), which is too short to be detected by EPR. At lower temperatures the NO adsorption complexes become accessible to EPR spectroscopy (Figs. 2–4) and give rise to the typical anisotropic signal at $g \approx 2.0$. However, the limited lifetime of the adsorption complexes is still manifested in the temperature-dependent homogeneous line broadening of their EPR signals (Figs. 5–7). The extracted homogeneous linewidths follow an Arrhenius behavior and different activation energies E_A of the adsorbed NO for the three systems H-ZSM-5, Na-ZSM-5, and Na-A were obtained (Table 1). These activation energies have to be interpreted as a local desorption energy per surface site. Two overlapping activated processes were found for H-ZSM-5, where we identified the process with $E_A = 20.2$ kJ/mol dominating at higher temperatures with the desorption of the NO molecules from the adsorption sites. The second process with $E_A = 1.1$ kJ/mol is only significant for $T < 90$ K and will not be discussed further. The activation energies follow the relation $E_A(\text{Na-ZSM-5}) < E_A(\text{Na-A}) \ll E_A(\text{H-ZSM-5})$ in accordance with the expected strong Lewis acidity of the aluminum defect centers (true Lewis sites) and the weak Lewis acid properties of the alkali metal cations (*3, 25*). This means that NO probe molecules are more strongly bound at aluminum defect centers than at Na^+ cations. The measured desorption temperatures $T_{\text{des}}(\text{silicalite}) < T_{\text{des}}(\text{Na-ZSM-5}) < T_{\text{des}}(\text{H-ZSM-5})$ for the different ZSM-5 zeolites support this result (Table 1). Again the highest value of T_{des} was found for H-ZSM-5. The pure silicalite sample gives rise to a significantly lower value T_{des} in comparison with the Na-ZSM-5 and H-ZSM-5 system because it has no Lewis acid centers acting as adsorption sites for NO. Nevertheless, the complete adsorption of nitric oxide for $T \leq 150$ K indicates the existence of weak adsorption sites that are presumably formed by electric surface fields in pores of the silicalite crystals.

The magnitude of the determined activation energies E_A and the low desorption temperatures are typical for a physisorption of the NO probe molecules at the Na^+ cations or aluminum defect centers. Thus the NO molecules are weakly bound to the Lewis acid adsorption sites where the bonding is caused by their electron pair acceptor properties.

These electron pair acceptor properties of the Lewis acid sites lead to a redistribution of the electron density within the adsorbed nitric oxide molecules (*25*). In this model the electronic structure of NO is assumed to be composed of a mixture of two resonance structures (*12*)

$$\underset{\mathbf{I}}{:\dot{\mathrm{N}}{=}\ddot{\mathrm{O}}:} \leftrightarrow \underset{\mathbf{II}}{:\ddot{\mathrm{N}}^{-}{=}\dot{\mathrm{O}}:^{+}}$$

Upon adsorption of the NO and coordination via its nitrogen to the acid site the contribution of the resonance structure **II** to the total electronic structure is enhanced due to the electron pair acceptor property of the Lewis acid site L^{n+} (*4*)

$$L^{n+} - :\ddot{\mathrm{N}}^{-}{=}\dot{\mathrm{O}}:^{+}.$$

This results in a shift of the unpaired spin density in the $^2\Pi_y^*$ NO molecular orbital toward the oxygen atom. Consequently, the nitrogen hf coupling decreases with rising electron pair acceptor strength of the Lewis acid site. The nitrogen hf coupling data in Table 1 support this model. The resulting relation $A_{yy}^{\text{N}}(\text{H-ZSM-5}) < A_{yy}^{\text{N}}(\text{Na-A}) < A_{yy}^{\text{N}}(\text{Na-ZSM-5})$ shows that the aluminum defect centers (true Lewis acid sites) in the H-ZSM-5 zeolite possess a higher electron pair acceptor strength or Lewis acidity than the sodium cations in the Na-A and Na-ZSM-5 zeolites in accordance with the determined activation energies E_A for the desorption processes.

Structure of the true Lewis acid sites. The nature of the aluminum defect centers is controversially discussed in the literature (*29–31*). In general extraframework aluminum species are assumed to act as true Lewis acid sites. On the basis of EPR results (*5, 21*) the most likely species are AlO^+ or Al^{3+}. Unfortunately, the EPR data in our work and also in previously published papers are not sufficient to determine precisely the structure of the NO adsorption complexes at the aluminum defect centers. It may also be possible that two Lewis acid site types exist simultaneously. The use of "intensity correction factors" u_{zz} which influence the g_{zz} region of the EPR spectrum (*23*) indicates the coexistence of two Lewis site types. A proof is still lacking and by our point of view it needs to be done by the inclusion of the EPR active NO dimer complexes which also may occur during adsorption (*8*). It will not be possible in this work to decide about the specific nature of the true Lewis acid site and we can only summarize the arguments supporting either AlO^+ or Al^{3+}.

The obtained aluminum shf coupling data alone would support the assignment of the aluminum defect centers to a trivalent aluminum ion. For an Al^{3+}–NO complex we would expect that its electronic properties are comparable with those of a Na^{+}–NO complex. A pulsed ENDOR study of the Na^{+}–NO adsorption complex in Na-A zeolites (*5*) revealed an almost entirely ionic bonding between the NO and the cation with a low spin density of $\rho_{3s}^{Na} = 0.9\%$ in the sodium 3*s* orbital. If we naturally assumed the same spin density in the 3*s* aluminum orbital for an Al^{3+}–NO complex we would obtain an isotropic aluminum shf coupling $A_{iso}^{Al} = 35$ MHz (*32*) in satisfactory accordance with the experimentally determined value A_{yy}^{Al} in Table 1. The relatively large total linewidths $\delta^{total}B_{xx} = 5.0$ mT and $\delta^{total}B_{zz} = 8.0$ mT obtained for the *x* and *z* direction in the simulations of the experimental spectra may also account for unresolved isotropic ^{27}Al shf couplings of such a magnitude.

An alternative way of distinguishing between AlO^{+} and Al^{3+} is given by a determination of the parameters l, E, and Δ from the principal values of the $\boldsymbol{g}$ tensor according to Eq. [2]. These equations are only valid in the limit of an ionic host crystal (*8, 19, 20*) and predict an orthorhombic $\boldsymbol{g}$ tensor. But the experimental data of NO adsorbed in H-ZSM-5 provide an axial-symmetric tensor within the accuracy of the spectral analysis $g_{xx} - g_{yy} \leq 0.0002$. The application of Eq. [2] gives an unreasonably large or even infinite energy splitting E between the $^2\Sigma^*$ and $^2\Pi_y^*$ NO molecular orbitals. Such conditions indicate a significant covalent bonding contribution in the adsorption complex (*19, 23*). However, if we take into account only first-order interactions (*6*) we can deduce a rough estimate for the $^2\Pi_x^* - {}^2\Pi_y^*$ splitting of the NO molecular orbitals of about $\Delta \approx 0.137$ eV and a covalency parameter $l \approx 0.34$ from the formula of g_{zz} and the first term in the equations for $g_{xx/yy}$ (Eq. [2]). It is worth noting that the admixture of the next higher $^3\Sigma$, $^3\Sigma^*$ molecular states into the wavefunction of the $^2\Pi_y^*$ ground state should be taken into account in a more rigorous analysis of the $\boldsymbol{g}$ tensor principal values. Nevertheless, the estimated covalency parameter $l \approx 0.34$ deviates strongly from the typical ionic bonding case with $l \approx 1$ (*19*) in contradiction with the ionic character of a possible Al^{3+}–NO species. Moreover the energy splitting $\Delta \approx 0.137$ eV is close to the value $\Delta \approx 0.165$ eV that has been determined for NO coordinated to monovalent sodium cations in zeolite Na-ZSM-5 (*23*). In the case of an Al^{3+}–NO complex we would expect an approximately three times larger value for the $^2\Pi_x^* - {}^2\Pi_y^*$ splitting (*2*). Thus, the $\boldsymbol{g}$ tensor data are more in favor of an assignment of a true Lewis acid site to an AlO^{+} extraframework species than to a trivalent aluminum ion.

In the case of an AlO^{+}–NO adsorption complex we can only speculate about the origin of the relatively large isotropic aluminum shf coupling because only the A_{yy}^{Al} value could be resolved by EPR. In a simple molecular orbital picture of an AlO^{+} species the aluminum 3*s* atomic orbitals would not contribute to its molecular valence orbitals in any case. Therefore, a simple spin density transfer from the $^2\Pi_y^*$ NO orbital to the Al 3*s* orbitals is not likely to explain the substantial isotropic ^{27}Al shf interaction. This leaves only spin polarization effects as a possible source for the aluminum shf data. ^{27}Al pulsed ENDOR spectra of NO adsorbed at aluminum defect centers in H-ZSM-5 zeolites have been interpreted in terms of a negative isotropic shf coupling $A_{iso}^{Al} = -29$ MHz (*5*) and support this explanation. An approximated Al–N bond distance was determined in (*5*) by using aluminum shf coupling values.

CONCLUSIONS

The overall adsorption–desorption properties of NO probe molecules in zeolite materials can be studied by the EPR signal of the paramagnetic $^2\Pi_{3/2}$ molecular state of desorbed NO in the gas phase. The measurement of the temperature dependence of this EPR signal provides the opportunity to define a specific desorption temperature T_{des} at which desorption of NO molecules into the gas phase becomes detectable. These desorption temperatures are characteristic quantities for the adsorption strength of the zeolite with respect to nitric oxide. The information gained is basically the same as that for conventional temperature-controlled desorption experiments and related techniques. Quantitative data about the acidity of the specific Lewis sites in terms of desorption energies can be obtained by an analysis of the temperature-dependent homogeneous line broadening of the EPR signal of NO adsorption complexes at temperatures below T_{des}. The temperature dependence of the homogeneous linewidths follows an Arrhenius law and allows an evaluation of the activation energy E_A of NO at the specific Lewis acid sites in a microscopic manner. We have to note that this activation energy is the equivalent of a desorption energy and describes the local behavior per single NO adsoprtion complex. An alternative microscopic way to qualitatively determine the acidity of the Lewis sites in terms of their electron pair acceptor strength is given by the measurement of the nitrogen hf couling in the NO adsorption complex. Here an increasing acidity results in a decreasing A_{yy}^{N} principal value of the $\boldsymbol{A}^{N}$ hf coupling tensor.

For the investigated materials the highest acidity was found for the aluminum defect centers in H-ZSM-5 zeolites by all three methods. The activation energy of NO at these true Lewis acid sites ($E_A = 20.2$ kJ/mol) is significantly higher in comparison with the data obtained for weak Lewis acid sites such as sodium cations in zeolites Na-A ($E_A = 7.1$ kJ/mol) and Na-ZSM-5 ($E_A = 4.1$ kJ/mol). The qualitative order of the electron pair acceptor strengths of these adsorption sites deduced from the nitrogen hf coupling is in accordance with the measured activation energies. The stronger bond of the NO with the aluminum defect centers is also indicated by the covalent bond contributions as deduced from the $\boldsymbol{g}$ tensor values and the relatively large aluminum shf coupling. However, it is not possible to assign unambiguously the true Lewis acid sites to either Al^{3+} or AlO^{+} species on the basis of the EPR results. This might become feasible by way of an improved analysis of the $\boldsymbol{g}$ tensor of the true Lewis site–NO adsorption complex in combination with an

experimental determination of the sign of the aluminum shf interaction. For instance, ^{27}Al–^{14}N triple-resonance and quantum chemical modeling of the complex structure may well lead to a more conclusive result.

The desorption temperatures determined by gas-phase EPR are consistent with the obtained activation energies for the zeolite system ZSM-5, T_{des}(H-ZSM-5) > T_{des}(Na-ZSM-5) > T_{des}(silicalite). The silicalite material does not possess Lewis acid sites. Thus, it shows the lowest value T_{des} and the EPR signal of the adsorbed NO state cannot be observed. It seems to be surprising that a lower desorption temperature T_{des} was found for Na-A than for Na-ZSM-5 because E_A(Na-A) > E_A(Na-ZSM-5). This indicates that the local desorption behavior of the probe molecules at a specific Lewis acid site may deviate from the overall adsorption/desorption properties of the zeolite. Therefore, if the acidity of different Lewis sites is characterized by means of the measurement of the desorption temperatures the same zeolite host materials should be used. Otherwise, the actual activation energies and nitrogen hf couplings should be determined for the formed NO adsorption complexes because the methods used probe the actual local properties at the adsorption site.

EPR spectroscopy is a versatile tool for investigating the adsorption–desorption behavior of NO probe molecules in zeolites and thereby provides an opportunity for studying the acidity of Lewis sites in these materials. The advantage of the EPR method is that it allows a microscopic characterization of the structure of the formed NO adsorption complex and of the nature of the specific Lewis acid adsorption sites.

ACKNOWLEDGMENTS

This work has been supported by the DFG within the Sonderforschungsbereich SFB 294, Project F7 Moleküle in Wechselwirkung mit Grenzflächen, and Professor D. Michel for helpful discussions. We thank Professor A. Gutsze for providing the Na-A type zeolite.

REFERENCES

1. W. E. Addison and R. M. Barrer, *J. Chem. Soc*., 757–769 (1955).
2. P. H. Kasai and R. J. Bishop Jr., "Electron Spin Resonance Studies of Zeolite Chemistry and Catalysis" (J. A. Rabo, Ed.), ACS Monograph 171, pp. 350–391, Am. Chem. Soc., Washington, DC (1976).
3. A. Gutsze, M. Plato, F. Witzel, and H. G. Karge, *Stud. Surf. Sci. Catal*. **98,** 71–72 (1994).
4. A. Pöppl, T. Rudolf, P. Manikandan, and D. Goldfarb, *J. Am. Chem. Soc*. **122,** 10194–10200 (2000).
5. A. Pöppl, T. Rudolf, and D. Michel, *J. Am. Chem. Soc*. **120,** 4879–4880 (1998).
6. J. H. Lunsford, *J. Chem. Phys*. **46,** 4347–4351 (1967); J. H. Lunsford, *J. Phys. Chem*. **72,** 2141–2144 (1968).
7. J. H. Lunsford, *J. Phys. Chem*. **72,** 4163 (1968).
8. H. Yahiro, A. Lund, R. Aushu, N. P. Benetics, and M. Shiotani, *J. Phys. Chem. A* **104,** 7950–7956 (2000).
9. T. Rudolf, A. Pöppl, W. Brunner, and D. Michel, *Magn. Reson. Chem*. **37,** S93–S99 (1999).
10. G. Herzberg, "Molecular Spectra and Molecular Structure," 2nd ed., von Nostrand, New York (1953).
11. R. Beringer and J. G. Castle Jr., *Phys. Rev.* **78,** 581–586 (1950).
12. G. C. Dousmanis, *Phys. Rev.* **97,** 967–970 (1955).
13. H. Margenau and A. Henry, *Phys. Rev.* **78,** 587–592 (1950).
14. J. J. Gallagher, F. D. Bedard, and C. M. Johnson, *Phys. Rev.* **93,** 729–733 (1954).
15. R. A. Frosch and H. M. Foley, *Phys. Rev.* **88,** 1337–1349 (1952).
16. H. E. Radford, *Phys. Rev.* **122,** 114–130 (1961).
17. H. E. Radford, *Phys. Rev.* **126,** 1035–1045 (1962).
18. P. J. Moht and B. N. Taylor, *J. Phys. Chem. Ref. Data* **28,** 1713–1852 (1999).
19. H. R. Zeller and W. Känzig, *Helv. Phys. Acta* **40,** 845–872 (1967); W. Känzig and H. R. Zeller, *Helv. Phys. Acta* **40,** 873–886 (1967).
20. C. L. Gardner and M. A. Weinberger, *Can. J. Chem*. **48,** 1317–1322 (1970).
21. A. Gutsze, M. Plato, H. G. Karge, and F. Witzel, *J. Chem. Soc. Faraday Trans*. **92,** 2495–2498 (1996).
22. T. C. James and R. J. Thibault, *J. Chem. Phys*. **41,** 2806–2813 (1964).
23. T. Rudolf, A. Pöppl, W. Hofbauer, and D. Michel, *Phys. Chem. Chem. Phys*. **3,** 2167–2173 (2001).
24. N. G. van Kampen, "Stochastic Processes in Physics and Chemistry," North-Holland Personal Library, Amsterdam (1992).
25. K. Ulbricht and P. Köhler, *Z. Chem*. **25,** 253–254 (1985).
26. G. T. Kokotailo, S. L. Lawton, D. H. Olson, and W. Meier, *Nature* **272,** 437–438 (1978).
27. R. W. Thompson and M. J. Huber, *J. Cryst. Growth* **56,** 711–722 (1982).
28. D. Wang and G. R. Hanson, *Appl. Magn. Reson*. **11,** 401–415 (1996).
29. G. H. Kühl, *J. Phys. Chem. Solids* **38,** 1259 (1977).
30. H. G. Karge, *Stud. Surf. Sci. Catal*. **65,** 133–156 (1991) .
31. H. Pfeifer, *NMR Basic Prin. Prog*. **31,** 31–90 (1994).
32. J. R. Morton and K. F. Preston, *J. Magn. Reson*. **30,** 577–582 (1978).